

Monocular and Hybrid Analysis for TA×4 Fluorescence Detectors

Yuki Kusumori,^{a,*} Yuichiro Tameda,^a Shoichi Ogio,^b Keitaro Fujita,^b
Yoshiki Tsunesada,^c Takashi Sako,^b Shoma Sato,^a Yutaro Takagi,^a Kohei Komori,^a
Hirai Iwagami^a and for the Telescope Array Collaboration

^aGraduate School of Engineering, Osaka Electro-Communication University, Neyagawa-shi, Osaka
572-8530, Japan

^bInstitute for Cosmic Ray Research, Kashiwa-no-ha 5-1-5, Kashiwa city, Japan

^cOsaka Metropolitan University, sugimoto-ku, oosaka 558-8585, Japan

E-mail: me23a006@oecu.jp

The TA×4 project is an extension of the Telescope Array (TA) experiment, aimed at clarifying the origin of the highest energy cosmic rays. It has deployed 4 fluorescence detectors (FDs) and 130 surface detectors (SDs) at the northeast lobe of the original TA array and 8 FDs and 127 SDs at the southeast lobe of the original TA array, expanding the detection area about four times larger than the TA experiment. This expansion enables us to sample larger data. The TA×4 has been collecting data to obtain solid evidence of the excess of events in the arrival direction distribution, known as the TA hotspot, reported in 2014 by the TA experiment. The north and south observations began in 2018 and 2019, respectively, and are ongoing except for a hiatus from February to June 2020 due to the COVID-19 pandemic. In this presentation, we will report the details of TA×4 FD monocular analysis.

38th International Cosmic Ray Conference (ICRC2023)
26 July - 3 August, 2023
Nagoya, Japan



*Speaker

1. Introduction

The TA×4 experiment is an extension of the Telescope Array (TA) experiment by a factor of 4 in its observation area, with the goal of revealing the origin and nature of the highest energy cosmic rays. The TA×4 experiment is collecting data to obtain solid evidence for an intermediate scale anisotropy of arrival direction distribution of cosmic rays with energies greater than 5.7×10^{19} eV, the so-called TA hotspot, which was reported by the TA collaboration in 2014 [1].

Currently, 4 fluorescence detectors (FDs) and 130 surface detectors (SDs) are deployed north-east of the TA Middle Drum (MD) station, and 8 FDs and 127 SDs are deployed southeast of TA Black Rock Mesa (BRM) station. As a result of these deployments, the observation area, which includes the TA SD array, is approximately 2.5 times larger than the area covered by the TA SD array alone.

The TA×4 SDs are arranged in a square grid pattern at 2.08 km intervals, which is wider than the original TA SD spacing of 1.2 km, suitable for detecting secondary particles induced by a primary cosmic ray with energy greater than 3×10^{19} eV. The TA×4 Northern FDs at MD station (TA×4FD@MD) observe the sky 3° – 17° in elevation and 12° – 76° in azimuth clockwise from North overlooking the Northern TA×4 SD array, and the TA×4 Southern FDs at BRM station (TA×4FD@BRM) view the sky with the same elevation and azimuth angles of 238° – 350° clockwise from North, overlooking the TA×4 Southern SD array.

The atmospheric fluorescence light generated by the air shower is focused by a spherical mirror with an aperture of ~ 2.3 m and imaged by a photomultiplier tube (PMT) camera at the focal point. The camera's array of PMTs has a light sensitive area of 690 mm wide \times 580 mm tall and the camera optically obscures an area of 750 mm \times 635 mm in front of the mirror. The PMTs in the camera are hexagonal with a flat-to-flat dimension of 42 mm. A 16×16 (256 in total) close-packed array of these PMTs makes up the image sensor of the camera, with each PMT covering a 1° field of view [2]. The spherical mirrors are reconditioned ones from the previous HiRes experiment [3].

The TA×4FD@MD and TA×4FD@BRM started observations in June 2018 and October 2019, respectively, and have been observed regularly except for a pause from February to June 2020 due to the COVID-19 pandemic. In this study, we generate Monte-Carlo (MC) events and investigate the accuracy of TA×4 FD monocular and hybrid reconstructions. We also compared the accuracy of the FD monocular and hybrid analyses.

2. Fluorescence Detector Monocular Analysis

To ensure an accurate measurement of the flux of ultra-high energy cosmic rays (UHECRs), it is crucial to properly calculate the acceptance of detectors. To this end, we employ the Monte-Carlo Method to simulate both the interactions of cosmic rays in the atmosphere and the response of the detectors.

2.1 Monte-Carlo Simulations

The air shower simulation uses the CORSIKA code [4], which can simulate the interaction and trajectory of air shower particles. We used QGSJET II-04 as a hadronic interaction model [5], assuming protons as the primary particles of UHECRs. The number of photons incident onto the

FD is estimated from the air shower generated according to the particle species and energy of the primary cosmic rays. The detector simulation uses the obtained photon counts to create waveform data considering the structure of each FD. Note that the detector simulation accurately reproduces the position of the telescope and shielding by structures.

The simulation conditions for TA×4FD@MD and TA×4FD@BRM monocular analysis are summarized in Table 1.

Table 1: Monte-Carlo simulation conditions for monocular analysis

particle type	proton
energy	$\log_{10}(E/\text{eV}) = 19.0, 19.5, 20.0$
Number of event	5000
Zenith	0–65°
Azimuth	0–360°
Shower generator	CORSIKA (QGSJET II-04)

2.2 Reconstruction and Resolution Studies

Monocular reconstruction is a method to determine the development of air showers of primary cosmic ray particles using the signal waveform and time of photons incident onto each PMT of a single FD station. First, PMT sorting is performed to remove noise such as noctilucence. Next, the Shower-Detector Plane (SDP) is determined from the trajectory of photons captured by the PMT camera, and the geometry is reconstructed from the time of photon incidence. Finally, the obtained geometry is used to reconstruct the longitudinal development, taking into account the amount of energy loss in the atmosphere.

Once the event reconstruction is complete, it is crucial to eliminate poorly reconstructed events prior to computing any physics outcomes. For the monocular reconstruction, we adopted selection criteria described in Table 2.

Table 2: TA×4 Monocular selection criteria

Quality Cuts
Number of PMTs used for reconstruction > 15
$X_{\text{start}} > 10 \text{ g/cm}^2$
$X_{\text{start}} < X_{\text{max}} < X_{\text{end}}$

We investigated the accuracy of the monocular reconstruction by using MC events that passed the selection criteria. The reconstructed values were compared to the initial thrown parameters for each MC event. Figure 1 shows the resolutions of impact parameter (R_p), the slope of the shower axis in the SDP (ψ), X_{max} , and energy in the case of $\log_{10}(E/\text{eV}) = 19.0$. Figure 1 shows the resolutions of each parameters obtained by the monocular reconstruction of TA×4FD@BRM. Table 3 summarizes the results for each FD station for three energies: $10^{19.0}$ eV, $10^{19.5}$ eV, and $10^{20.0}$ eV. The resolutions of R_p and ψ show no energy-dependent tendencies. However, the resolutions of

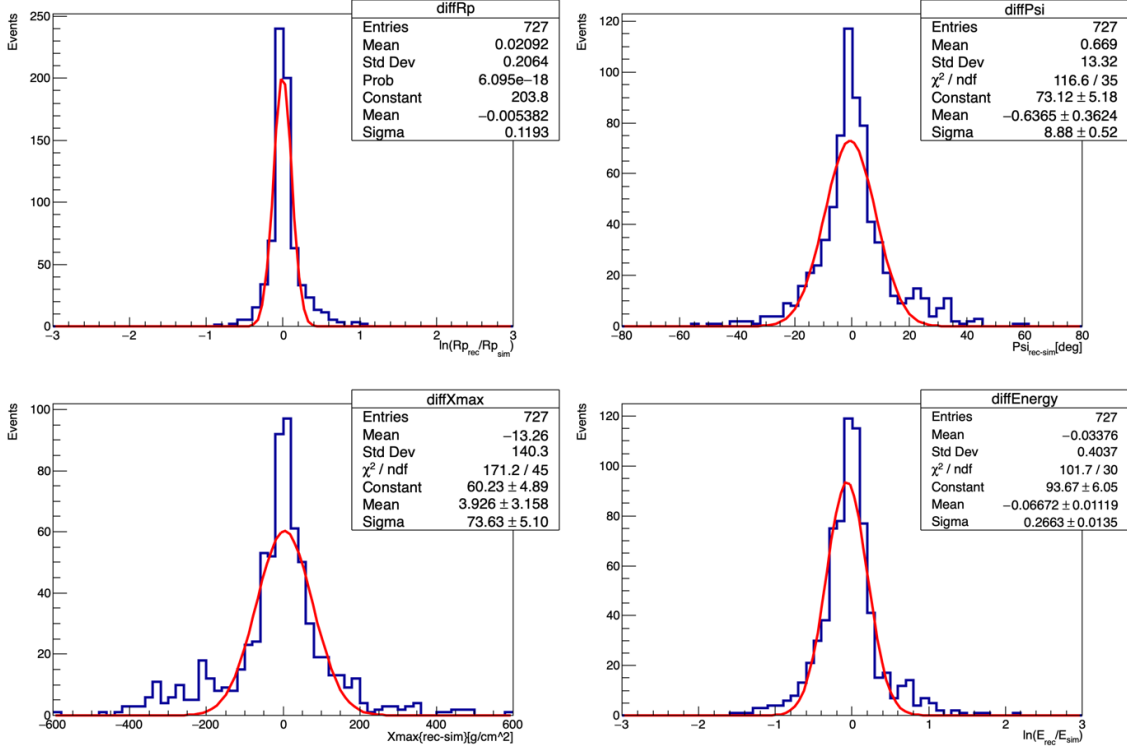


Figure 1: Resolutions of R_p , ψ , X_{\max} , and energy for Monte-Carlo events reconstructed by monocular analysis for TA×4FD@BRM at $\log_{10}(E/\text{eV}) = 19.0$. The red curves are Gaussian fits.

X_{\max} and energy appear to have energy-dependent tendencies. The biases tend to be opposite for MD and BRM. We will conduct further investigations into these energy-dependent tendencies.

Table 3: Accuracy of monocular reconstruction for each energy

Location	Energy	ΔR_p [%]	$\Delta \Psi$ [degree]	ΔX_{\max} [g/cm ²]	ΔE_0 [%]
TA×4FD@MD	$10^{19.0}$ eV	0.0 ± 11.2	0.2 ± 7.9	0 ± 76	-4.2 ± 25
	$10^{19.5}$ eV	0.1 ± 9.3	0.3 ± 6.6	8 ± 79	-6 ± 25
	$10^{20.0}$ eV	-0.3 ± 9.0	-0.4 ± 7.5	21 ± 117	-11 ± 42
TA×4FD@BRM	$10^{19.0}$ eV	-0.8 ± 8.9	-0.5 ± 12.0	4 ± 74	-7 ± 27
	$10^{19.5}$ eV	-0.2 ± 9.6	0.7 ± 9.5	-3 ± 90	-5 ± 35
	$10^{20.0}$ eV	0.4 ± 8.7	1.4 ± 7.2	-22 ± 107	-11 ± 27

3. Hybrid Analysis

3.1 TA×4 Hybrid Analysis

The TA×4 experiment observes air showers by using FD and SD, and the analysis using data measured by both FD and SD is called hybrid analysis. The hybrid analysis requires SD simulations in addition to FD simulations. The SD simulation takes into account the actual trigger conditions

and calibration data. Then, the GEANT4 [6] is used to calculate the energy and the energy loss in the scintillator in the upper and lower layers. The simulation also takes into account the exterior of the antenna and solar panels, etc.

3.2 Monte-Carlo Simulations

Since the hybrid analysis uses both FD and SD information, we generate new MC events as summarized in Table 4.

Table 4: Monte-Carlo simulation conditions for hybrid analysis

Simulation conditions	Proton
Energy	$\log_{10}(E/\text{eV}) = 19.0, 19.5, 20.0$
Zenith	0–70°
Azimuth	0–360°
Shower generator	CORSIKA (QGSJET II-04)

3.3 Reconstruction and Resolution Studies

Hybrid reconstruction incorporates the timing information measured by a SD as well as information from a PMT camera that detects photons in the monocular FD. Initially, the SDP is determined following the same procedure as in monocular analysis. The geometry of the air shower is then reconstructed using the timing information of the SDs that detect air shower particles near its core position, which constrain the geometry of the air shower. Using this geometry, we reconstruct the air shower longitudinal development and determine the air shower development of primary cosmic ray particles.

The selection criteria for the hybrid analysis is given in Table 5. Figure 2 shows the resolutions of R_p , ψ , X_{max} , and energy in the case of $\log_{10}(E/\text{eV}) = 19.0$. Table 6 summarizes for accuracy of hybrid reconstruction for each FD station for three energies: $10^{19.0}$ eV, $10^{19.5}$ eV, and $10^{20.0}$ eV. The results do not show any energy-dependent tendencies.

Table 5: TA×4 Hybrid selection criteria

Quality Cuts
$X_{\text{start}} < X_{\text{max}} < X_{\text{end}}$
Zenith > 75 deg
No saturated PMT at FD

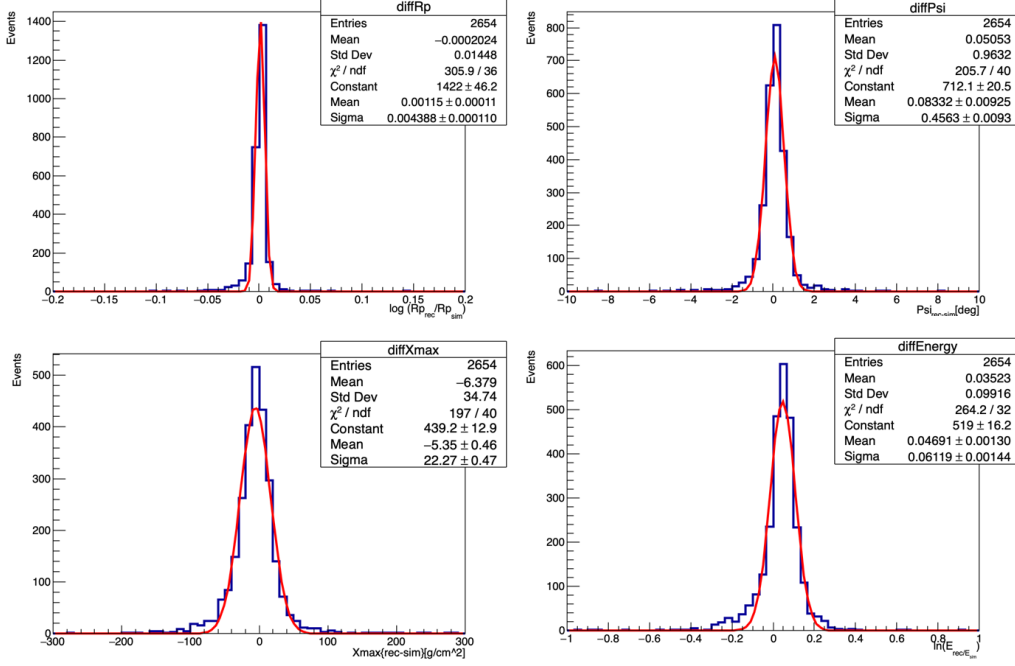


Figure 2: Resolutions of R_p , ψ , X_{\max} , and energy for Monte-Carlo events reconstructed by hybrid analysis for TA×4FD@BRM at $\log_{10}(E/eV) = 19.0$. The red curves are Gaussian fits.

Table 6: Accuracy of hybrid reconstruction for each energy

Location	Energy	ΔR_p [%]	$\Delta \Psi$ [degree]	ΔX_{\max} [g/cm ²]	ΔE_0 [%]
TA×4FD@MD	$10^{19.0}$ eV	0.1 ± 6.0	0.1 ± 0.6	-5 ± 30	4.5 ± 8.9
	$10^{19.5}$ eV	0.1 ± 0.5	0.2 ± 0.4	-6 ± 24	0.1 ± 1.3
	$10^{20.0}$ eV	0.0 ± 0.1	0.3 ± 0.3	-8 ± 17	0.3 ± 6.0
TA×4FD@BRM	$10^{19.0}$ eV	0.1 ± 0.4	0.1 ± 0.4	-5 ± 22	4.7 ± 0.6
	$10^{19.5}$ eV	0.4 ± 2.7	0.1 ± 0.3	-4 ± 17	3.2 ± 5.3
	$10^{20.0}$ eV	0.1 ± 0.4	0.2 ± 0.3	-7 ± 15	1.7 ± 5.7

4. Comparisons of Monocular and Hybrid Analysis

Figure 3 compares the biases and resolutions of TA×4FD@MD and TA×4FD@BRM monocular and hybrid reconstructions. The hybrid analysis adds the information of the SDs that detected the charged particles arriving at the ground surface, which improves the geometric reconstruction of the air shower compared to the FD monocular reconstruction. For all energy levels, the hybrid reconstruction consistently shows better resolutions than those of the monocular reconstruction.

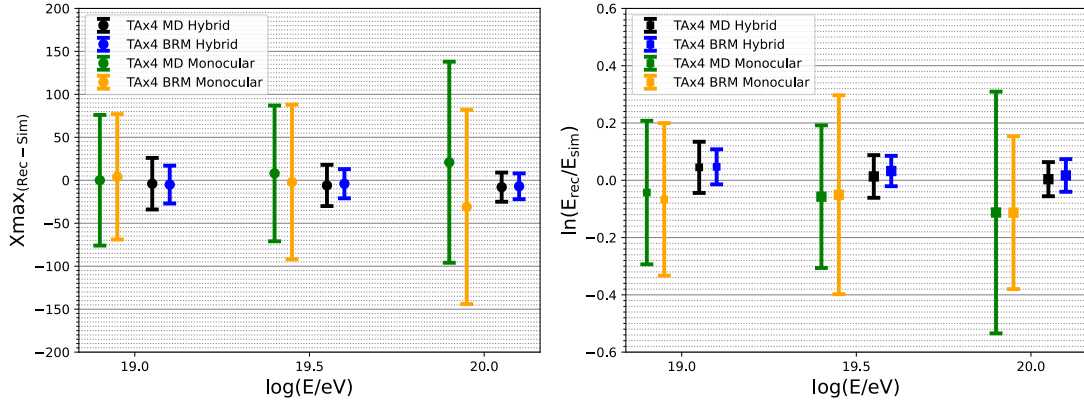


Figure 3: $(X_{\max})_{rec} - (X_{\max})_{sim}$ and $\ln(E_{rec})/(E_{sim})$ vs. $\log_{10}(E/eV)$. The left panel shows the comparisons of biases and resolutions of X_{\max} for $\log_{10}(E/eV) = 19.0, 19.5,$ and 20.0 for monocular and hybrid reconstructions, and the right panel shows those of the energy. The error bars indicate the 1σ standard deviations by Gaussian fitting.

5. Data Analysis

We conducted a hybrid analysis using observed data obtained from the TA×4 experiment. The data acquisition periods were from October 2019 to October 2022 for TA×4FD@MD and from July 2020 to October 2022 for TA×4FD@BRM. Figure 4 shows an event display of one event of data.

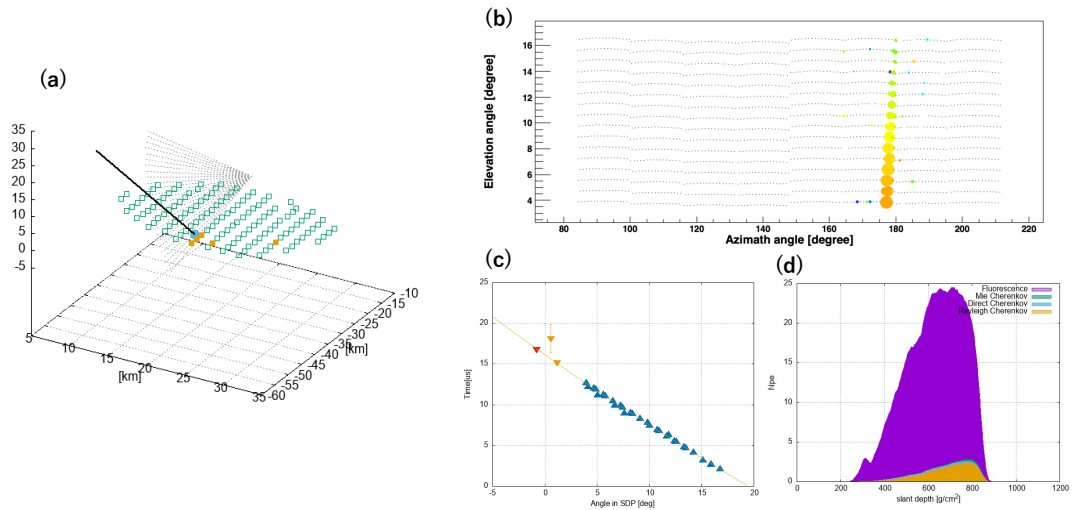


Figure 4: Event display. (a) Air shower observed by SD and FD. (b) The number of photoelectrons captured by the PMT of the FD is shown, and the color indicates the timescale. (c) The blue triangle makers are FD PMT timing and inverted triangle are SD timing. The red inverted triangle is a detector which is used in analysis. (d) Reconstructed shower profile with relative contributions of fluorescence light, Cherenkov light.

6. Summary and Plan

The TA×4 experiment aims to reveal the origin and nature of the highest energy cosmic rays and has expanded its observation area with 12 new FDs and 257 new SDs. The TA×4FD@MD and TA×4FD@BRM started stable observations in June 2018 and October 2019, respectively. In this study, we performed Monte-Carlo simulations and event reconstructions using both monocular and hybrid analysis for TA×4FD@MD and TA×4FD@BRM. By assessing the reconstruction performance, we concluded that the hybrid analysis yielded better resolutions compared to the monocular analysis. We also analyzed the observed data by the hybrid reconstruction.

We will investigate the underlying factors contributing to the disparity in resolutions of TA×4FD@BRM and TA×4FD@MD monocular reconstructions. Also, we will continue to analyze the observed data and conduct the Data/MC comparisons. Then, we will measure the TA×4 hybrid energy spectrum.

References

- [1] R.U. Abbasi *et al.*, *Astrophysical Journal Letters*, **790**, L21 (2014).
- [2] M. Potts for the Telescope Array Collaboration, *PoS ICRC2021* (2021) 395.
- [3] G.D. Furlich (2020) [Doctoral dissertation, The University of Utah].
- [4] D. Heck, J. Knapp, J. Capdevielle, G. Schatz and T. Thouw, *Tech. Rep. FZKA 6019* (1998).
- [5] S. Ostapchenko, *Physical Review D* **83**, 014018 (2011).
- [6] J. Allison *et al.*, *Nuclear Instruments and Methods in Physics Research Section A: Accelerators, Spectrometers, Detectors and Associated Equipment* **835**, 186 (2016).

Full Authors List: Telescope Array Collaboration

R.U. Abbasi¹, Y. Abe², T. Abu-Zayyad^{1,3}, M. Allen³, Y. Arai⁴, R. Arimura⁴, E. Barcikowski³, J.W. Belz³, D.R. Bergman³, S.A. Blake³, I. Buckland³, B.G. Cheon⁵, M. Chikawa⁶, A. Fedynitch^{6,7}, T. Fujii^{4,8}, K. Fujisue⁶, K. Fujita⁶, R. Fujiwara⁴, M. Fukushima⁶, G. Furlich³, Z. Gerber³, N. Globus⁹, W. Hanlon³, N. Hayashida¹⁰, H. He⁹, R. Hibi², K. Hibino¹⁰, R. Higuchi⁹, K. Honda¹¹, D. Ikeda¹⁰, N. Inoue¹², T. Ishii¹¹, H. Ito⁹, D. Ivanov³, A. Iwasaki⁴, H.M. Jeong¹³, S. Jeong¹³, C.C.H. Jui³, K. Kadota¹⁴, F. Kakimoto¹⁰, O. Kalashev¹⁵, K. Kasahara¹⁶, S. Kasami¹⁷, S. Kawakami⁴, K. Kawata⁶, I. Kharuk¹⁵, E. Kido⁹, H.B. Kim⁵, J.H. Kim³, J.H. Kim^{3†}, S.W. Kim¹³, Y. Kimura⁴, I. Komae⁴, K. Komori¹⁷, Y. Kusumori¹⁷, M. Kuznetsov^{15,18}, Y.J. Kwon¹⁹, K.H. Lee⁵, M.J. Lee¹³, B. Lubsandorzhiiev¹⁵, J.P. Lundquist^{3,20}, T. Matsuyama⁴, J.A. Matthews³, J.N. Matthews³, R. Mayta⁴, K. Miyashita², K. Mizuno², M. Mori¹⁷, M. Murakami¹⁷, I. Myers³, S. Nagataki⁹, K. Nakai⁴, T. Nakamura²¹, E. Nishio¹⁷, T. Nonaka⁶, S. Ogio⁶, H. Ohoka⁶, N. Okazaki⁶, Y. Oku¹⁷, T. Okuda²², Y. Omura⁴, M. Onishi⁶, M. Ono⁹, A. Oshima²³, H. Oshima⁶, S. Ozawa²⁴, I.H. Park¹³, K.Y. Park⁵, M. Potts^{3‡}, M.S. Pshirkov^{15,25}, J. Remington³, D.C. Rodriguez³, C. Rott^{3,13}, G.I. Rubtsov¹⁵, D. Ryu²⁶, H. Sagawa⁶, R. Saito², N. Sakaki⁶, T. Sako⁶, N. Sakurai⁴, D. Sato², K. Sato⁴, S. Sato¹⁷, K. Sekino⁶, P.D. Shah³, N. Shibata¹⁷, T. Shibata⁶, J. Shikita⁴, H. Shimodaira⁶, B.K. Shin²⁶, H.S. Shin⁶, D. Shinto¹⁷, J.D. Smith³, P. Sokolsky³, B.T. Stokes³, T.A. Stroman³, Y. Takagi¹⁷, K. Takahashi⁶, M. Takamura²⁷, M. Takeda⁶, R. Takeishi⁶, A. Taketa²⁸, M. Takita⁶, Y. Tameda¹⁷, K. Tanaka²⁹, M. Tanaka³⁰, S.B. Thomas³, G.B. Thomson³, P. Tinyakov^{15,18}, I. Tkachev¹⁵, H. Tokuno³¹, T. Tomida², S. Troitsky¹⁵, R. Tsuda⁴, Y. Tsunesada^{4,8}, S. Udo¹⁰, F. Urban³², I.A. Vaiman¹⁵, D. Warren⁹, T. Wong³, K. Yamazaki²³, K. Yashiro²⁷, F. Yoshida¹⁷, Y. Zhezher^{6,15}, and Z. Zundel³

¹ Department of Physics, Loyola University Chicago, Chicago, Illinois 60660, USA

² Academic Assembly School of Science and Technology Institute of Engineering, Shinshu University, Nagano, Nagano 380-8554, Japan

³ High Energy Astrophysics Institute and Department of Physics and Astronomy, University of Utah, Salt Lake City, Utah 84112-0830, USA

⁴ Graduate School of Science, Osaka Metropolitan University, Sugimoto, Sumiyoshi, Osaka 558-8585, Japan

⁵ Department of Physics and The Research Institute of Natural Science, Hanyang University, Seongdong-gu, Seoul 426-791, Korea

⁶ Institute for Cosmic Ray Research, University of Tokyo, Kashiwa, Chiba 277-8582, Japan

⁷ Institute of Physics, Academia Sinica, Taipei City 115201, Taiwan

⁸ Nambu Yoichiro Institute of Theoretical and Experimental Physics, Osaka Metropolitan University, Sugimoto, Sumiyoshi, Osaka 558-8585, Japan

⁹ Astrophysical Big Bang Laboratory, RIKEN, Wako, Saitama 351-0198, Japan

¹⁰ Faculty of Engineering, Kanagawa University, Yokohama, Kanagawa 221-8686, Japan

¹¹ Interdisciplinary Graduate School of Medicine and Engineering, University of Yamanashi, Kofu, Yamanashi 400-8511, Japan

¹² The Graduate School of Science and Engineering, Saitama University, Saitama, Saitama 338-8570, Japan

¹³ Department of Physics, SungKyunKwan University, Jang-an-gu, Suwon 16419, Korea

¹⁴ Department of Physics, Tokyo City University, Setagaya-ku, Tokyo 158-8557, Japan

¹⁵ Institute for Nuclear Research of the Russian Academy of Sciences, Moscow 117312, Russia

¹⁶ Faculty of Systems Engineering and Science, Shibaura Institute of Technology, Minato-ku, Tokyo 337-8570, Japan

¹⁷ Graduate School of Engineering, Osaka Electro-Communication University, Neyagawa-shi, Osaka 572-8530, Japan

¹⁸ Service de Physique Théorique, Université Libre de Bruxelles, Brussels 1050, Belgium

¹⁹ Department of Physics, Yonsei University, Seodaemun-gu, Seoul 120-749, Korea

²⁰ Center for Astrophysics and Cosmology, University of Nova Gorica, Nova Gorica 5297, Slovenia

²¹ Faculty of Science, Kochi University, Kochi, Kochi 780-8520, Japan

²² Department of Physical Sciences, Ritsumeikan University, Kusatsu, Shiga 525-8577, Japan

²³ College of Science and Engineering, Chubu University, Kasugai, Aichi 487-8501, Japan

²⁴ Quantum ICT Advanced Development Center, National Institute for Information and Communications Technology, Koganei, Tokyo 184-8795, Japan

²⁵ Sternberg Astronomical Institute, Moscow M.V. Lomonosov State University, Moscow 119991, Russia

²⁶ Department of Physics, School of Natural Sciences, Ulsan National Institute of Science and Technology, UNIST-gil, Ulsan 689-798, Korea

²⁷ Department of Physics, Tokyo University of Science, Noda, Chiba 162-8601, Japan

²⁸ Earthquake Research Institute, University of Tokyo, Bunkyo-ku, Tokyo 277-8582, Japan

²⁹ Graduate School of Information Sciences, Hiroshima City University, Hiroshima, Hiroshima 731-3194, Japan

³⁰ Institute of Particle and Nuclear Studies, KEK, Tsukuba, Ibaraki 305-0801, Japan

³¹ Graduate School of Science and Engineering, Tokyo Institute of Technology, Meguro, Tokyo 152-8550, Japan

³² CEICO, Institute of Physics, Czech Academy of Sciences, Prague 182 21, Czech Republic

Acknowledgements

The Telescope Array experiment is supported by the Japan Society for the Promotion of Science(JSPS) through Grants-in-Aid for Priority Area 431, for Specially Promoted Research JP21000002, for Scientific Research (S) JP19104006, for Specially Promoted Research JP15H05693, for Scientific Research (S) JP19H05607, for Scientific Research (S) JP15H05741, for Science Research (A) JP18H03705, for Young Scientists (A) JPH26707011, and for Fostering Joint International Research (B) JP19KK0074, by the joint research program of the Institute for Cosmic Ray Research (ICRR), The University of Tokyo; by the Pioneering Program of RIKEN for the Evolution of Matter in the Universe (r-EMU); by the U.S. National Science Foundation awards PHY-1806797, PHY-2012934, PHY-2112904, PHY-2209583, and PHY-2209584 as well as AGS-1613260, AGS-1844306, and AGS-2112709; by the National Research Foundation of Korea (2017K1A4A3015188, 2020R1A2C1008230, & 2020R1A2C2102800); by the Ministry of Science and Higher Education of the Russian Federation under the contract 075-15-2020-778, IISN project No. 4.4501.18, by the Belgian Science Policy under IUAP VII/37 (ULB), by National Science Centre in Poland grant 2020/37/B/ST9/01821. This work was partially supported by the grants of the joint research program of the Institute for Space-Earth Environmental Research, Nagoya University and Inter-University Research Program of the Institute for Cosmic Ray Research of the University of Tokyo. The foundations of Dr. Ezekiel R. and Edna Wattis Dumke, Willard L. Eccles, and George S. and Dolores Doré Eccles all helped with generous donations. The State of Utah supported the project through its Economic Development Board, and the University of Utah through the Office of the Vice President for Research. The experimental site became available through the cooperation of the Utah School and Institutional Trust Lands Administration (SITLA), U.S. Bureau of Land Management (BLM), and the U.S. Air Force. We appreciate the assistance of the State of Utah and Fillmore offices of the BLM in crafting the Plan of Development for the site. We thank Patrick A. Shea who assisted the collaboration with much valuable advice and provided support for the collaboration's efforts. The people and the officials of Millard County, Utah have been a source of steadfast and warm support for our work which we greatly appreciate. We are indebted to the Millard County Road Department for their efforts to maintain and clear the roads which get us to our sites. We gratefully acknowledge the contribution from the technical staffs of our home institutions. An allocation of computing resources from the Center for High Performance Computing at the University of Utah as well as the Academia Sinica Grid Computing Center (ASGC) is gratefully acknowledged.

* Presently at: University of California - Santa Cruz

† Presently at: Argonne National Laboratory, Physics Division, Lemont, Illinois 60439,USA

‡ Presently at: Georgia Institute of Technology, Physics Department, Atlanta, Georgia 30332,USA